JOINT EUROPEAN TORUS JET

JET–P(85)24

R.J. Bickerton
and B.E. Keen

Tokamak Experiments

Tokamak Experiments

R.J. Bickerton
and B.E. Keen

JET-Joint Undertaking, Culham Science Centre, OX14 3DB, Abingdon, UK

Preprint of Paper to be published in the Proceedings of the Course and
Workshop on Basic Physical Processes of Toroidal Fusion Plasmas
(Varenna, Italy; 26 August – 3 September 1985)

In these lectures, the confinement principles of the tokamak are outlined and the present status of tokamak research is reviewed, with particular reference to the JET machine, which is the largest operating tokamak in the world. The need for additional heating in tokamaks is discussed and the various methods are compared. Certain parameter limitations (e.g. disruptions, sawtooth oscillations, impurities and a limits) presently encountered are detailed and options for surmounting these problems are presented. Their effect on energy confinement and the various empirical scaling laws encountered in differing conditions are discussed, particularly the confinement degradation observed in additional heating situations. Finally, the main achievements and future outlook with tokamaks are summarised.

ABSTRACT.

In these lectures, the confinement principles of the tokamak are outlined and the present status of tokamak research is reviewed, with particular reference to the JET machine, which is the largest operating tokamak in the world. The need for additional heating in tokamaks is discussed and the various methods are compared. Certain parameter limitations (e.g. disruptions, sawtooth oscillations, impurities and a limits) presently encountered are detailed and options for surmounting these problems are presented. Their effect on energy confinement and the various empirical scaling laws encountered in differing conditions are discussed, particularly the confinement degradation observed in additional heating situations. Finally, the main achievements and future outlook with tokamaks are summarised.

1 INTRODUCTION

The tokamak is a particular magnetic confinement system, pioneered in the Soviet Union and one of a class of so-called closed-line confinement systems designed to contain a hot plasma having isotropic pressure. By the late 1960's/early 1970's, it became clear that hot plasma with relatively good thermal insulation from the walls was much more easily obtained with tokamak apparatus than with other systems (notably the pinch and the stellarator). Consequently, in the last fifteen years, there has been world-wide concentration on tokamak experiments. As the size of apparatus has increased, remarkable progress has been made in increasing the two key (Lawson) parameters $\langle \hat{n}_i \hat{\tau}_E \rangle$ and $\hat{T}_i$ which measure progress towards a power generating fusion reactor. Here $\hat{n}_i$ is the ion density, $\hat{\tau}_E$ the energy confinement time which characterises the thermal insulation of the plasma from the material walls and $\hat{T}_i$ is the central ion temperature. [Typically, for a D-T reaction, the Lawson criteria require $\langle \hat{n}_i \hat{\tau}_E \rangle = 3 \times 10^{20} m^{-3} s$ and $\hat{T}_i = 10 keV$].

In these lectures, the confinement principles of the tokamak will be outlined together with the plasma behaviour expected on the basis of simple theoretical models. As will be seen, the plasma behaviour in experiments is in many respects strikingly different from that predicted and much is still not understood.

Wherever possible in this article we use JET details and JET results to illustrate the points being made. By this means we hope to both educate the student and inform the expert.

Definitive reviews of tokamak research have been given by Artsimovich (1972) and Furth (1972) and (1981).

As a potential reactor system the tokamak has three serious defects:

(i) It is a low β system, where β is the ratio of plasma to magnetic pressure. Since the power output per unit volume is proportional to β^2, the low β tends to lead to relatively large systems with a high cost per unit output. By shaping the plasma cross-section,

and other geometric modifications, it may be possible to overcome this problem;

(ii) Since it is a toroidal (doughnut-shaped) system with interleaved coils, vacuum vessel, etc., there are formidable problems in remote maintenance of such an active assembly;

(iii) In its basic form the tokamak is a pulsed system with the consequent problems of thermal cycling of components. Schemes for conversion into a steady-state system exist and some have been demonstrated. Nevertheless, there is concern that steady-state operation may require an excessive fraction of circulating power.

2 CONFINEMENT PRINCIPLES

The aim is to confine a hot, dense plasma away from a material wall for a sufficiently long period for fusion reactions to occur. Thus, an equilibrium configuration is needed in which the plasma pressure decreases outwards, i.e. one with a nested set of constant pressure surfaces enclosing a hot central plasma core. Such an equilibium must be maintained for many transit times at sound speeds across the system. (Note that for a fusion plasma the sound speed $[(T_e/M_i)^{1/2}]$ is ~ 10^6m/s so that the transit time for a system of dimension 1m is 1μs.)

The fact that plasma is a good conductor of electricity (~ 30 times better than copper at fusion temperatures) is used to hold the plasma in equilibrium through the interaction of the current density $\bar{j}$ with the local magnetic field $\bar{B}$. The equilibrium equation is then

$$\bar{j} \times \bar{B} = \nabla p \qquad (1)$$

where p is the plasma pressure (Spitzer, 1956).

By inspection of this equation, it is seen that on the nested constant pressure surfaces of the plasma, everywhere,

$$\bar{B}_n = 0 \qquad (2)$$

$$\bar{B} \neq 0$$

Here $\bar{B}_n$ is the component of magnetic field normal to the constant pressure surface. Since div $\bar{B} = 0$, it follows from a theorem of Poincarré (1881) that the only surfaces on which these properties can exist are topologically toroidal. The tokamak is a particular case of these toroidal equilibria. It has the special features of toroidal symmetry and a relatively strong externally generated toroidal field.

The essential tokamak geometry is shown in Fig. 1. The magnetic field components required for a symmetric equilibrium solution of Eq.1. are the self field (B_θ) of a toroidal current carried in the plasma itself and a "vertical field" (B_z) to hold the current carrying ring in major radius equilibrium. The tokamak is distinguished by having an additional very strong toroidal magnetic field B_ϕ generated by currents in external coils encircling the plasma cross section. The overall result of these three field components is a set of nested magnetic surfaces corresponding to the constant pressure surfaces. These magnetic surfaces are generated by multiple transits round the symmetry axis by magnetic field lines which follow a helical path, spiralling about a circular axis in the toroid. In general, the stronger the toroidal field component the more stable is the plasma equilibrium against gross instabilities. A safety factor q is defined as the number of times a field line encircles the major symmetry axis in traversing once around the minor axis, (i.e. to rotate through 2π in the poloidal (θ) direction.) For a magnetic surface with a circular cross-section in the meridional plane:

$$q_\psi = \frac{a^2}{2R} \frac{B_\phi}{I_p} \qquad (3)$$

where a and R are the minor and major radii of the magnetic surface, B_ϕ is the toroidal field component and I_p the toroidal current inside the surface. The surface is labelled by the poloidal flux ψ between the surface and the magnetic axis. The magnetic axis is the circle on to which the magnetic surfaces converge as $a \to 0$. The tokamak system can be <u>defined</u> as having

$$q_\psi > 1 \qquad (4)$$

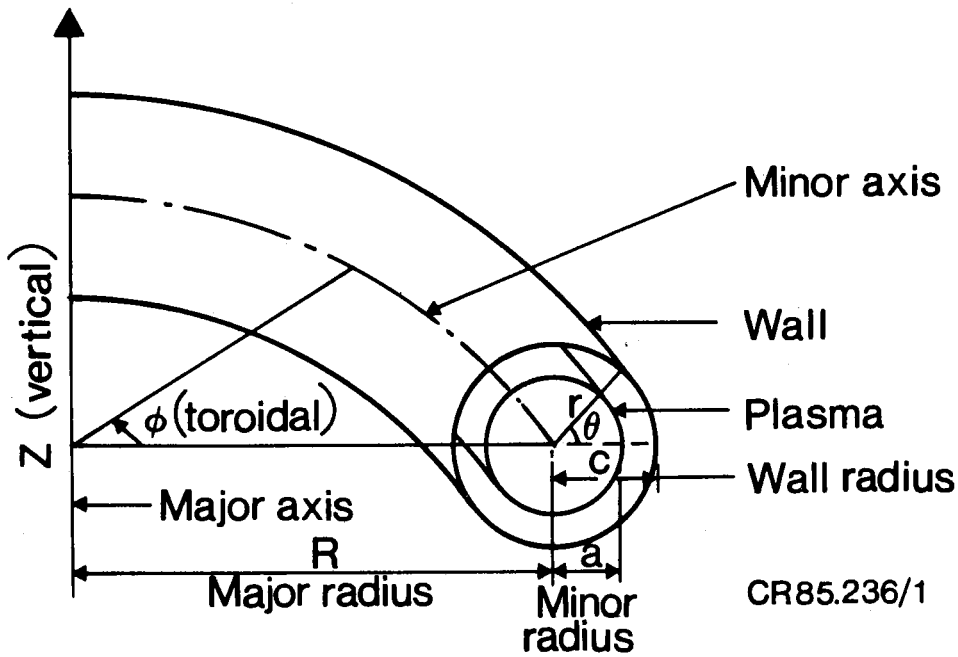

Fig. 1 Tokamak geometry.

P(85)24

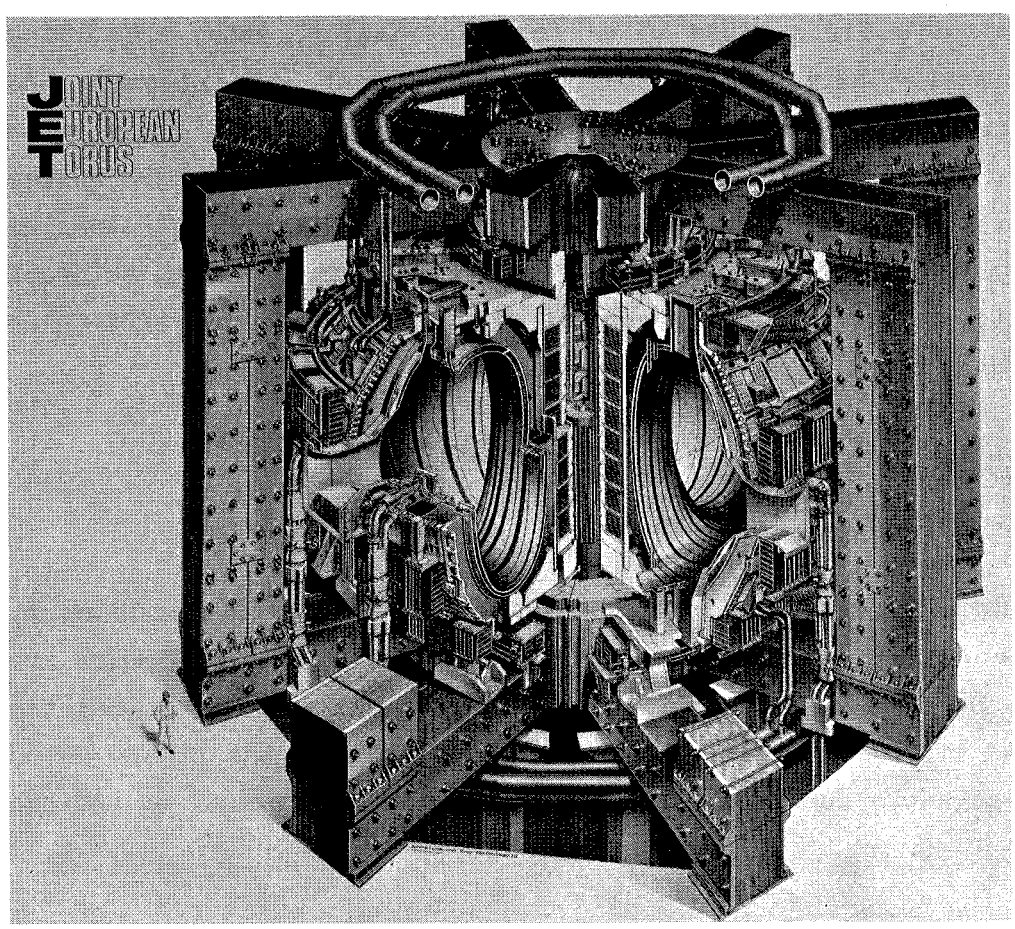

Fig. 2 Schematic diagram of the JET tokamak device.

P(85)24

everywhere in the plasma. (Systems with $q_\psi < 1$ at all radii are classified as toroidal pinches and generally have more restrictive requirements for stability).

Combining the relation,

$$\text{curl } \bar{B} = 4\pi\bar{j} \tag{5}$$

with Eq.(1) and applying these to this set of toroidal nested surfaces leads to the Grad-Shafranov equilibrium equation, (Laing et al,1959)

$$x\frac{\partial}{\partial x}\left(\frac{1}{x}\frac{\partial\psi}{\partial x}\right) + \frac{\partial^2\psi}{\partial y^2} + ff' + x^2g' = 0 \tag{6}$$

where $x = R/R_0$, $y = z/R_0$, $p = (B_0^2/4\pi)g(\psi)$ and $B_\phi = (R_0B_0/R)f(\psi)$. Here R_0 is the major radius of the magnetic axis, B_0 the toroidal field component on the magnetic axis. This equation can be combined with equations for plasma heating and for plasma losses by transport processes to calculate the temporal evolution of plasma equilibria. The equation is also used to deduce from external magnetic measurements the details of the equilibrium inside experimental tokamaks.

It is important to note, that according to a theorem by Tamm (1958), charged particles are absolutely confined, that is from conservation of energy and angular momentum the orbit of a charged particle cannot depart from a magnetic surface by more than a distance Δ, where

$$\Delta = \frac{Mcv}{eB_\theta} \tag{7}$$

where M, v and e are the particle mass, velocity and charge. This is particularly important with respect to non-thermal particles such as α-particles created by thermonuclear reactions.

3 TOKAMAK DEVICE

The essential elements in a tokamak system are:

(i) a toroidal vacuum vessel;

(ii) external coils to produce a strong toroidal field inside the vacuum vessel;

(iii) external "poloidal coils" to produce the required field for major radius equilibrium of the plasma ring, to shape the plasma cross-section and to hold it in equilibrium against displacements parallel to the major axis;

(iv) a pulse transformer system to drive a toroidal current in the plasma;

(v) power supplies to drive the required currents in the various coils.

Fig. 2 shows schematically the JET tokamak device which is at present the largest such machine in the world. It has been built and is being operated through the collaborative efforts of the countries in the European Community plus Sweden and Switzerland. It is located at Culham near Abingdon in the United Kingdom. This machine is designed for plasmas with non-circular cross-section with the elongation (vertical radius(b)/horizontal radius(a)) ranging up to 1.6. The figure shows the essential features of a tokamak described above, that is the toroidal field coils, the toroidal vacuum vessel, the poloidal coils performing the functions of a primary winding, equilibrium windings and feedback windings. JET is unusual in having eight iron return limbs to carry the return flux from the primary windings. In operation, these limbs are unsaturated and serve to reduce the stray field both in the plasma volume and in the external region where diagnostic and neutral injection systems are mounted.

The principal engineering problems in tokamak design arise from the large magnetic forces acting on the toroidal field coils. For example, in the JET case (JET Report R-5, 1975), each one of the 32 coils has an inward force of ~ 1800 tonnes due to the toroidal field alone and a toppling torque of ~ 200 tonne.m due to the interaction between the current in the toroidal field coils and the vertical magnetic field produced by the poloidal coils. In JET, these forces and torques are taken on a central column and by a complex mechanical structure between the toroidal field coils. Other large machines use different solutions; in the USA, the TFTR machine has shear panels between the field coils, while in the Japanese JT-60 the torque is transmitted to the building by massive steel bracing.

TABLE 1

Representative Medium-Sized Tokamaks

Machine	Country	R(m)	a(m)	K	B(T)	I_p(MA)
T-3	USSR	1.0	0.17	1.0	2.5	0.1
PLT	USA	1.3	0.4	1.0	3.5	0.6
T-10	USSR	1.5	0.37	1.0	3.5	0.5
ASDEX	FRG	1.6	0.4	2.0	2.6	0.5
D III	USA	1.4	0.4	1.4 - 1.8	2.6	1.0
PDX	USA	1.4	0.4	1.0	2.4	0.5
FT	Italy	0.8	0.23	1.0	8.0	0.6
Alcator C	USA	0.64	0.16	1.0	12	0.8

R = Major radius of toroid

a = Minor "horizontal" radius of plasma

K = Elongation = vertical/horizontal radius of plasma

B = Toroidal field strength at plasma centre

I_p = Plasma current

There are now more than 70 tokamaks of various sizes in the world (World Survey of Major Activities in Controlled Fusion Research, 1982, IAEA, Vienna). Table 1 shows the parameters of a representative range of medium-sized apparatus. The Russian machine T-3 is listed as the pioneer machine in which relatively high electron temperatures (~1keV) and good energy confinement (~2ms) were first demonstrated. After T-3, the machines evolved in three directions. PLT and T-10 are natural successors to T-3, in that they have the same circular cross-section plasma bounded by a material diaphragm or limiter and they are just bigger. ASDEX, DIII and PDX are distinguished by being able to operate with a magnetic limiter or divertor. In these cases, the plasma boundary is a separatrix which separates closed toroidal magnetic surfaces from open ones. The machines FT and Alcator C represent a third line of evolution in which increased performance is obtained not by increasing the physical size but by increasing the magnitude of the toroidal magnetic field. In all these successor machines, the plasma current is increased over that used in T-3 by a factor x5 - 10, up to levels of 0.5 - 1.0MA.

The parameters of large tokamaks, operating or under construction, are summarised in Table 2, (Little and Rawls, 1984); all are designed for currents well in excess of 1MA. In fact, JET has already operated at the full rated toroidal field (B_t = 3.5T) with the design plasma current of 5MA. Two of these machines, T-15 and Tore-Supra are partly technology experiments, since they use superconducting toroidal field coils; niobium/tin is used in T-15 and niobium/titanium for Tore-Supra. FT-U is the largest machine following the high magnetic field route. All these machines will have powerful systems for heating the plasma using multi-megawatts of different combinations of the main methods, i.e. neutral beam injection, ion cyclotron resonance, lower hybrid resonance and electron cyclotron resonance. By the early 1990's, these machines will have provided a wide range of experimental data on which to base further progress. Note that both JET and TFTR are designed to demonstrate significant α-particle heating of the plasma by operating in deuterium-tritium mixtures in the last stages of their programmes.

TABLE 2

Large Tokamak Parameters

Machine	Country	R(m)	a(m)	K	B(T)	I_p (MA)	Operating Gas	Discharge Duration(s)	First Operation
JET	EEC	2.96	1.25	1.6	3.5	5	H/D/D-T	10 - 20	June '83
TFTR	USA	2.55	0.85	1.0	5.2	2.5	H/D/D-T	1 - 3	Dec '82
JT-60	Japan	3.0	0.95	1.0	4.5	2.7	H	5 - 10	April '85
T-15	USSR	2.4	0.70	1.0	4.0	2.0	H	5	'86
TORE-SUPRA	France	2.4	0.70	1.0	4.5	1.7	H/D	30	'87
D IIID	USA	1.67	0.67	1 - 2	2.2	2 - 3	H	2 - 5	'86
FT-U	Italy	0.92	0.31	1.0	8.0	1.6	H/D	1.5	'87

4 PLASMA HEATING

Since the tokamak relies on a substantial current in the plasma to produce one of the magnetic field components essential for confinement, it also incorporates an automatic plasma heating method, namely Ohmic

heating, due to the finite resistivity of the plasma. The classical theory of plasma which includes binary (Coulomb) collisions between ions and electrons, but not instability phenomena, predicts that the resistivity η will fall as the electron temperature T_e rises (Spitzer, 1956), i.e.

$$\eta \propto T_e^{-3/2} \tag{8}$$

In tokamak experiments, the resistivity for current flow in the toroidal direction is one of the few transport coefficients (if not the only one) to agree with classical theory. Consequently, it follows both theoretically and experimentally that as the electron temperature rises so the power input from Ohmic heating falls. When the likely thermal insulation of the plasma is included in the calculation, it is found that, almost certainly, it is impossible to heat a tokamak plasma to thermonuclear temperatures by Ohmic heating alone. A possible exception is a tokamak with very high magnetic fields, i.e. those fields which are on the limit of engineering feasibility (B ~ 16T). In such machines, the plasma current density can be very high, increasing the Ohmic power density. For tokamaks with toroidal field strengths in the range 3-8 T, which are proto-typical of the eventual envisaged superconducting fusion reactor, additional plasma heating is essential.

By analogy with ordinary gases, the most obvious way to heat a plasma is to compress it. This is readily done either by increasing the toroidal magnetic field rapidly, or alternatively, and requiring much less power, to move the plasma rapidly to a smaller major radius where the toroidal field is stronger. Both these techniques have been variously tried (Bol et al (1974), Kaganski et al (1976), Cima et al (1976), Tait et al (1984), Goncharev et al (1984)). For the compression to be adiabatic, it must take place on a time-scale short compared with the characteristic time for energy loss from the system. In early experiments, frequently this was not the case but the techniques for plasma handling were demonstrated and marginal heating was seen. In more recent experiments, technical advances have permitted adequately fast compression, the electron density and ion temperature has increased as expected but there was an unexplained loss of electron energy.

Adiabatic compression has the disadvantages that it is by definition a transient heating method and that in the compressed state the plasma volume is small so that the utilisation of the expensive volume of toroidal magnetic field inside the coils is poor. Indeed, with some scaling laws for plasma confinement, better results could be obtained by using the whole of the available machine volume without adiabatic compression. As a result, adiabatic compression studies are now pursued more for their physical interest than as prototype heating methods for fusion reactors.

Consequently, most attention is now given to heating systems in which power in the form of high energy particles or RF waves is injected into a stationary plasma. The most successful of these techniques has been neutral injection in which beams of energetic neutral atoms (usually H or D) with energies in the range 20 - 80 keV are injected into the plasma. The energetic neutral particles pass freely across the confining magnetic fields into the plasma where they are ionised and trapped. Power levels up to 7MW have already been used in tokamak experiments (Kitsunezaki et al, 1984). The physical processes of fast-neutral ionisation, trapping and slowing down through Coulomb collisions have been shown to agree with orbit and binary collision theory. The technique depends entirely on the spectacular advances made in the last 15 years in ion-source, beam extraction and neutralisation technology. The method has the advantage that all the difficult technological problems are related to the injection system itself which is outside the tokamak torus.

The other main approach is to heat the plasma by the injection of RF power. In this case, antennae are required inside the torus to launch the waves, while the wave propagation and absorption inside the plasma itself is for most frequencies a complex and poorly understood physical process. Three main frequencies are in use, corresponding to resonances in the plasma interior:

(1) the ion cyclotron frequency ($\omega_{ci} = \frac{eB}{M_i c}$);

(2) the lower hybrid frequency

$$(\omega_{LH} = \left|\frac{\omega_{pi}^2\ \omega_{ce}\ \omega_{ci}}{\omega_{pi}^2 + \omega_{ce}\omega_{ci}}\right|^{\frac{1}{2}} \simeq \omega_{pi} >> \omega_{ci}\ );$$

(3) the electron cyclotron frequency ($\omega_{ce} = \frac{eB}{mc}$).

Here $\omega_{pi} = \left|\frac{4\pi ne^2}{M_i}\right|^{\frac{1}{2}}$ is the ion plasma frequency.

The aim is to launch a plasma wave towards the interior of the plasma at such a frequency that a resonance and correspondingly large absorption is encountered near the plasma centre. Typical frequencies for a tokamak such as JET with a deuterium plasma density of $\sim 10^{20} m^{-3}$ in a field of 3.5T are,

Ion cyclotron heating	25 - 55MHz
Lower hybrid heating	~ 1.5GHz
Electron cyclotron heating	~ 100GHz

In general, the difficulty and cost of generating high power rises with the frequency while the difficulty of launching and coupling to the plasma decreases with the frequency. The power levels used at present range from 5MW of ICRH (Jacquinot et al, 1985), ~ 1MW of Lower Hybrid Heating (Porkolab et al, 1984), and ~ 1MW of Electron Cyclotron Resonance Heating (Alikaev et al, 1984). The experimental results obtained with these methods on a variety of tokamaks will be discussed in a later section.

5 PLASMA DIAGNOSTICS

The measurement of plasma parameters is a challenging task since it is not possible to insert material measuring devices into the hot plasma. Thus the methods used depend either on analysing the radiation and particles leaving the plasma or measuring the plasma effects on beams of radiation or particles deliberately injected into or passed through the plasma.

Table 3 shows a list of the diagnostic systems installed or planned for the JET tokamak. The list is typical for modern machines although there is a greater emphasis on neutron diagnostics in view of the high performance and eventual D-T operation expected of this machine. By comparison with the diagnostics used nearly a decade ago (Bickerton 1977), it is noteworthy that there has been little advance in the techniques used. The main advances have been made in the engineering of systems for larger and potentially radioactive machines, in the in-service reliability, and in data-collection and analysis. Modern plasma diagnostics are well described in Stott et al (1982)

6 EXPERIMENTAL RESULTS

As a typical example of behaviour observed in the latest tokamak machines, this section concentrates on results obtained on JET, which is representative of the newer devices.

Figs. 3-5 show the basic parameters of current, loop voltage, density, electron temperature and ion temperature observed plotted as a function of time, as well as the T_e profile at different times in the pulse. These traces are all for the same plasma discharge (Pulse No. 5507). The sequence of events is as follows:

(i) Normally, the toroidal magnetic field is driven up by the power supplies to a pre-determined level and then held constant for the duration of the plasma current pulse. For special investigations, the plasma current rise can be initiated while the toroidal field is still rising;

(ii) the transformer is biased in one direction slowly, inducing a relatively low loop voltage around the torus;

(iii) the vacuum vessel is pulse-filled with hydrogen or deuterium gas to give an initial pressure of $10^{-5} \rightarrow 10^{-4}$ mbar;

(iv) a switch is opened in the primary circuit causing the current in the primary windings to fall towards zero, applying a voltage per turn in the range 10 - 20 V. This causes the gas to break down and the plasma current to rise, typically at the rate of 2MA/s for JET. The primary winding current is then driven negative at a

TABLE 3

JET DIAGNOSTICS

Plasma Parameter	Principal Diagnostic	Secondary Diagnostic
Current	External Rogowski coils Internal pick-up coils (18 in each octant)	
Loop volts	External flux loops	. Bolometry
Position and shape	External flux loops combined with internal pick-up coils	. Spectroscopy
Density	. Single chord 2mm μ-wave interferometer	. Thomson scattering
	. 7 vertical, 3 horizontal chord DCN laser (195μm) interferometer	
	. Microwave reflectometer	
	. Langmuir probes (sol)	
Electron Temperature	. Single point Thomson scattering (1Hz) multiple chord	. X-ray pulse height spectrometer
	. electron cyclotron emission (slow and fast) → $T_e(R,Z,t)$	
	. Lidar Thomson scattering ($T_e(R)$)	
Ion temperature	. Neutral particle profile analysis (4 chords)	. Neutron emission profile
	. Neutron yield	
	. Neutron spectrometers	
	. X-ray crystal spectrometer	
Z_{eff}	. Visible continuum emission 523.5nm	. Pulse Height
		. Spectrometer
		. Spectroscopy
		. Resistivity
Impurity content	. Quartz fibres (λ > 350nm)	. X-Ray Pulse
	. VUV survey spectrometer (10 - 170nm)	. Height spectrometer
	. 3 grazing-incidence spatial-scanning spectrometers (10 - 200nm)	
	. 1 spatial-scanning crystal spectrometer	
	. 1 active-phase crystal spectrometer	
Radiated power	. 1 bolometer in each Octant	. Spectroscopy and analysis
	. 3 bolometer cameras in one Octant (total of 34 chords)	
Neutral density.		. Neutral particle analyser
Reaction rate	. Neutron counters (BF_3 and fission)	
	. Foil activation	
Limiter (and antennae) temperature	. Infra-red cameras	
Fluctuations	. External flux loops	
	. Magnetic pick-up coils on the inside surface of the vacuum vessel	
	. Multi-chord soft X-ray cameras	
Limiter and wall interactions	. Langmuir & heat flux probes in plasma boundary	. Spectroscopy
	. Fast transfer system and surface analysis station (for exposure & intershot analysis of samples)	. Neutral particle analysis
Density, temperature and power flux in scrape-off layer	. Langmuir and heat-flux probes	
Plasma β	. Diamagnetic loop	. Equilibrium vertical field (b/a > 1.2)
		. Integration of plasma pressure over the volume

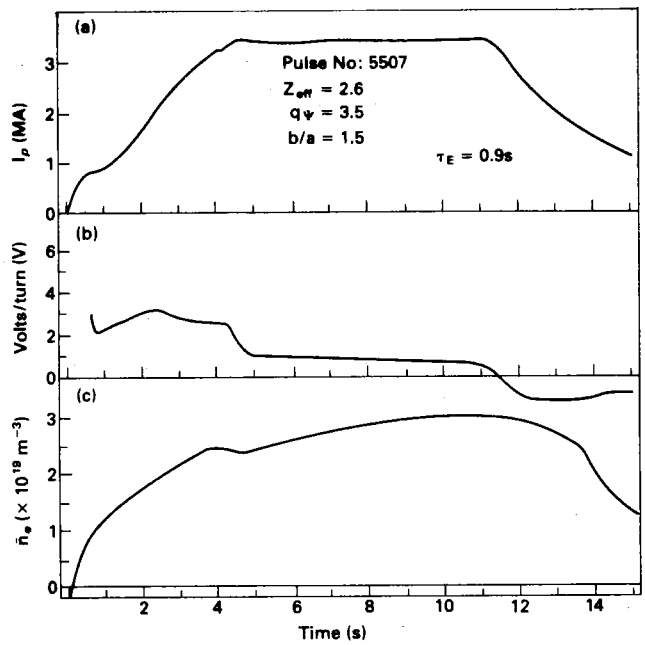

Fig. 3 Pulse No.5507: (a) Current, (b) Volts per turn and (c) Line average electron density versus time.

P(85)24

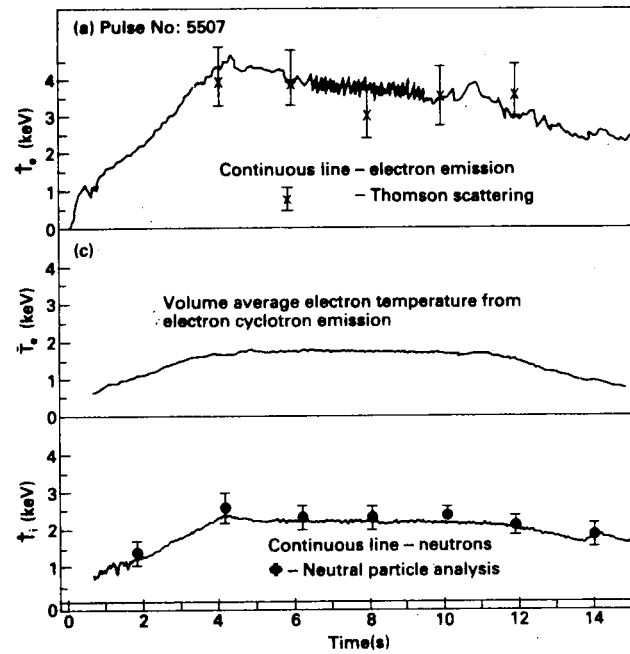

Fig. 4 Pulse No: 5507: (a) Peak electron temperature: (b) Volume averaged electron temperature (from ECE): (c) Peak ion temperature versus time.

P(85)24

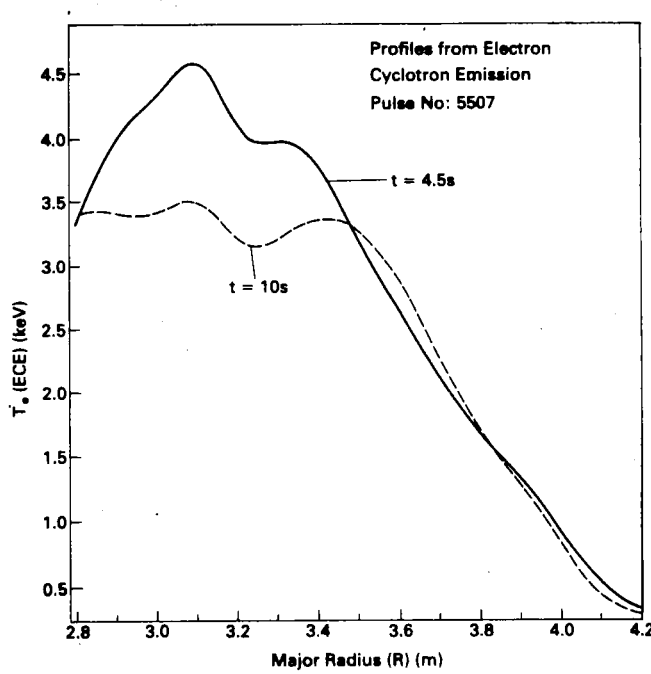

Fig. 5 Electron temperature (T_e) profiles, from ECE measurements, at t=4.5s and t=10s in Pulse No. 5507.

P(85)24

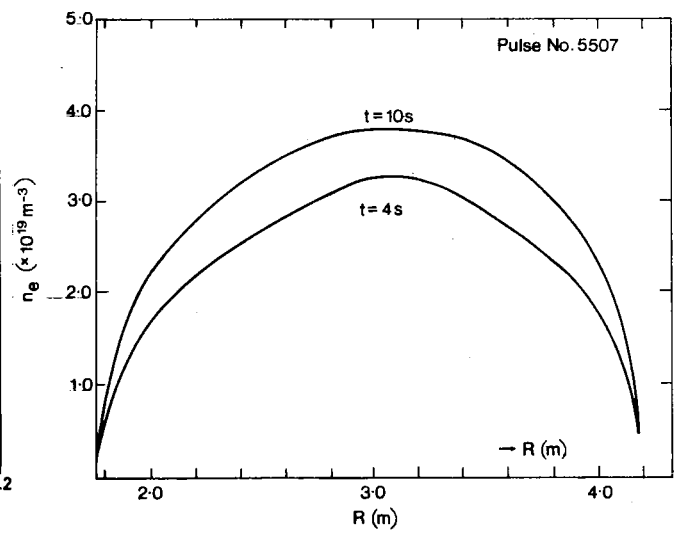

Fig. 6 Pulse No. 5507: Density profiles at t=4s and t=10s.

P(85)24

controlled rate to produce a slower current rise of ~ 1MA/s to the pre-set flat-top value. The current is held constant for some time (~ 5s on JET) and then ramped down to zero. For JET, no preionisation is used to assist the breakdown;

(v) after breakdown, more gas is bled into the torus at a feedback-controlled rate to give the desired plasma density variation with time.

To illustrate the orders of magnitude and the sequence of events, Figs. 3-7 show the time variation of basic plasma parameters in a 3.4 MA, Ohmic-heating only JET pulse. Fig. 3 shows the time variation of the plasma current (I_p), the voltage per turn (V_L) around the torus and the plasma electron density ($\bar{n}_e$) averaged over a chord though the plasma. Fig 4 shows on the first trace the electron temperature in the centre ($\hat{T}_e$) measured by electron cyclotron emission (ECE) and by Thomson scattering. The sampling rate is increased between 6.5 and 9.5s displaying the characteristic sawtooth temperature fluctuations due to an instability localised near the plasma centre. Note also the temperature peaking at 4.5keV at the start of the flat-top and falling later as the sawtooth instability flattens the radial temperature profile (Fig 5). The second trace in Fig. 4 shows that the volume average electron temperature ($\bar{T}_e$) reaches a plateau value of ~ 1.8keV. The third trace shows the central ion temperature ($\hat{T}_i$) deduced from neutron yield and from neutral particle analysis. This does not show such a strong early peaking in time as the electron temperature and has a plateau value ~ 2.2keV. Fig. 6 shows the electron density profile at two different times. Again, as with the electron temperature, the density profile flattens with time.

Fig. 7 shows the flux surfaces in the meridional plane calculated for the same discharge at various times. These are obtained by solving the Grad-Shafranov equation with parameterised pressure and current density profiles, the parameters are adjusted until the best fit is obtained to the measured fields and fluxes outside the plasma. The method determines the plasma boundary shape accurately, but the accuracy falls off for the surfaces in the plasma core.

These traces from JET serve to illustrate the magnitude and sequence of

events in a tokamak although timescales on smaller machines are typically an order of magnitude shorter and plasma currents are about five times smaller.

7 LIMITATIONS ON PLASMA PARAMETERS

It is found on all tokamaks that successful discharges without either gross instabilities or the excessive development of a non-thermal distribution of electrons (signalled by hard X-ray production) are limited to certain ranges of plasma density and plasma current, which in turn limits the electron and ion temperatures which can be reached and the energy confinement time which can be achieved. A normalised operating diagram representation has been developed by Hugill and Murakami which can be used for tokamaks of widely differing physical size and magnetic field strengths. The normalised current is represented by $1/q_{cyl}$ where

$$\frac{1}{q_{cyl}} = \frac{2\pi R}{A} \cdot \frac{I_p}{B_t} \qquad (9)$$

(A is the cross-sectional area of the plasma)
while the normalised density is $\bar{n}R/B_t$. Fig. 8 shows results from JET plotted on this normalised basis.

There are a number of physical processes (both predicted theoretically and observed experimentally) which limit the maximum parameters, achievable in tokamak plasmas. These processes are discussed in the following paragraphs.

(a) Disruptions

The tokamak disruption is a dramatic event in which plasma confinement is suddenly destroyed. In a major disruption, this is followed by a complete loss of current. This is illustrated in Fig. 9(a), which shows typical current disruptions observed in JET during the current rise, flat top and current fall periods of certain discharges. They pose a major threat in that they limit the range of operation in current and density, and their occurrence leads to large mechanical stresses and intense heat loads on the vessel.

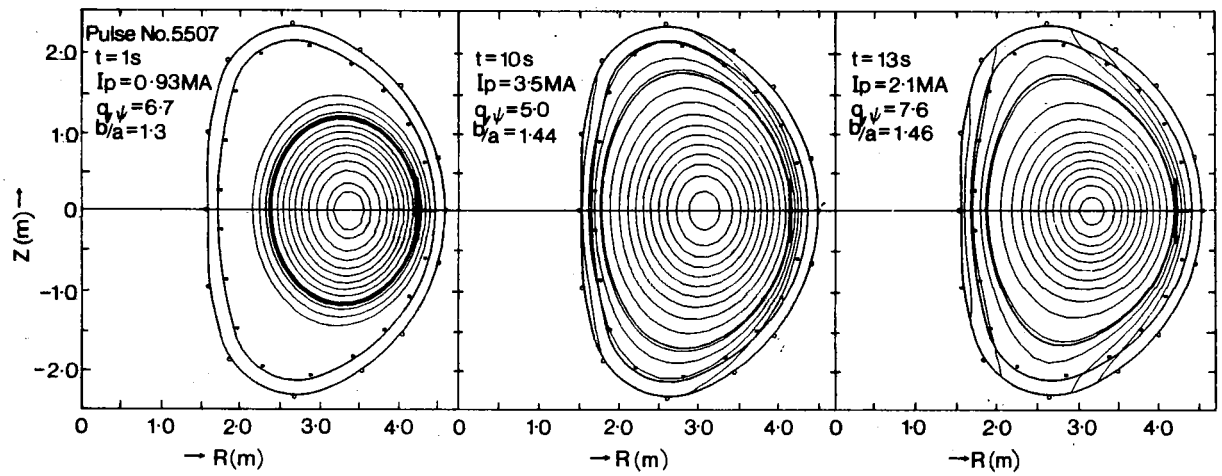

Fig. 7 Pulse No: 5507: Flux surfaces in the meridional plane calculated at (a) t=1s; (b) t=10s; and (c) t=13s.

P(85)24

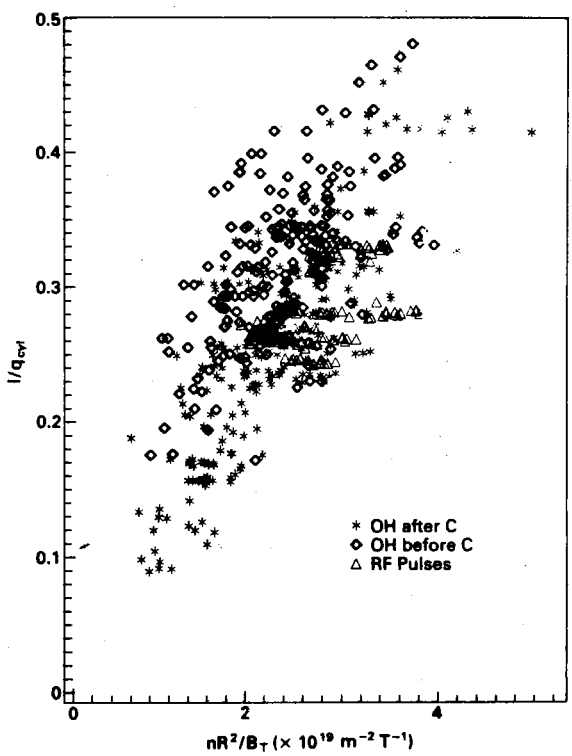

Fig. 8 Hugill-Murakami diagram of $1/q_{cyl}$ versus $\bar{n}R/B_T$ for ohmic plasmas before and after carbonisation and during ICRF heating.

P(85)24

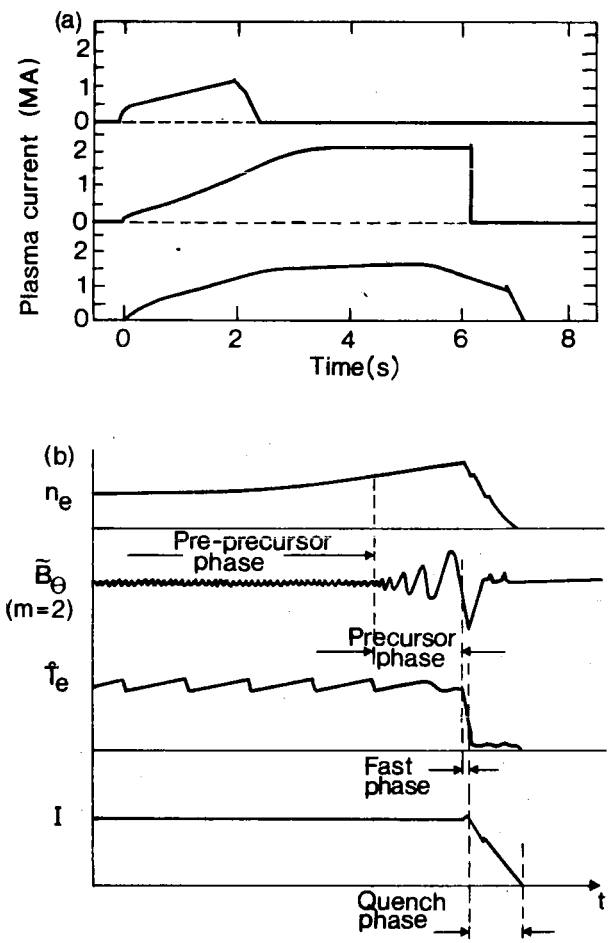

Fig. 9 (a) Current traces showing disruptions on the current rise flat-top and current fall during JET discharges; (b) typical time dependence of $m=2$ magnetic fluctuations $\tilde{B}_\theta$: central temperature and plasma current during the period of disruption. The disruption is precipitated by a density increase as shown.

P(85)24

The sequence of events is shown in Fig. 9(b). Essentially, there are four phases, as follows:

(i) Pre-precursor Phase: in which usually there is a change in the underlying conditions leading towards a more unstable configuration, such as an increase in total current or plasma density;

(ii) Precursor Phase: in which, following the underlying change, a critical point for the onset of MHD instability is reached and growth of m = 2 mode magnetic oscillations occurs (t = 10ms). (If m = 1 sawtooth oscillations (see Section 7(b)) are present prior to this stage, they are brought to a halt);

(iii) Fast Phase: in which, following considerable growth of the MHD instability, the central temperature collapses on a rapid timescale (~ 1ms) and a fast flattening of the radial current profile occurs;

(iv) Quench Phase: in which, the plasma current decays to zero with a decay time depending on particular conditions (decays of ~ 50MA/s have been observed in JET).

The operating region on JET is bounded on the high sides of both $\bar{n}R/B_t$ and $1/q$ by the disruptive instabilities (Fig. 8)

The physical processes involved are not well understood, and various models have been postulated to explain the observations. A plausible hypothesis is that, following the parameter changes in the pre-precursor phase leading to a more unstable configuration, tearing mode oscillations grow (particularly m = 2 modes) on the resonant surfaces q = m/n (i.e. 1/1, 2/1, 3/2, etc.). The magnetic islands produced grow rapidly with the oscillations and when these islands of different helicity have grown to the extent that they overlap, a region of ergodic field is created within the region of overlap. The surfaces are destroyed and plasma energy is lost rapidly by electron thermal conduction along field lines (the fast phase). The consequent central temperature collapse produces a fast flattening of the current profile. The current then decays rapidly to zero (quench phase).

Experience shows that the density limit depends on the plasma purity and on the power input. Fig. 10 shows the normalised results from other machines with both Ohmic heating and auxiliary heating. For Ohmic heating only, reducing the impurity content by gettering increases the density limit. A substantial increase in the limit is obtained when powerful additional heating is used. There is however some evidence of a universal density limit ($\bar{n}_c$) given by:

$$\bar{n}_c(m^{-3}) \simeq 2 \times 10^{20} B_t(T)/qR(m) \qquad (10)$$

Some experiments have exceeded this limit but only with discharges very prone to random disruptions during the heating phase. There is clearly a problem when with a given plasma density the current is ramped down, reducing 1/q, or when the additional heating is turned off at constant current. In the latter case, a disruption is inevitable unless the density can be reduced by special pumping panels as the power is reduced. In the case where the current is ramped down, the density falls due to a change in the recycling conditions at the wall. It is then simply a question of whether the density falls fast enough so that the discharge parameters stay on the right side of the limiting line in the Hugill diagram.

(b) Sawtooth Instabilities

Sawtooth oscillations of the electron temperature, T_e, are seen in most tokamaks; an example of these in JET (measured by ECE) is shown in Fig. 11. In the central plasma region, this periodic process shows a slow rise in electron temperature, on which m = 1 mode oscillations are superimposed, and then a fast drop in temperature occurs inside a certain radial region ($r<r_s$), and a steep rise is observed outside this radius. r_s is called the inversion radius. This gives rise to a fast flattening of the temperature profile. Fig. 5 shows an example of flattening of the temperature profile that results at later times in the JET discharge when sawteeth osciallations occur during the flat top (t = 10s).

A simple physical explanation of sawtooth behaviour has been suggested

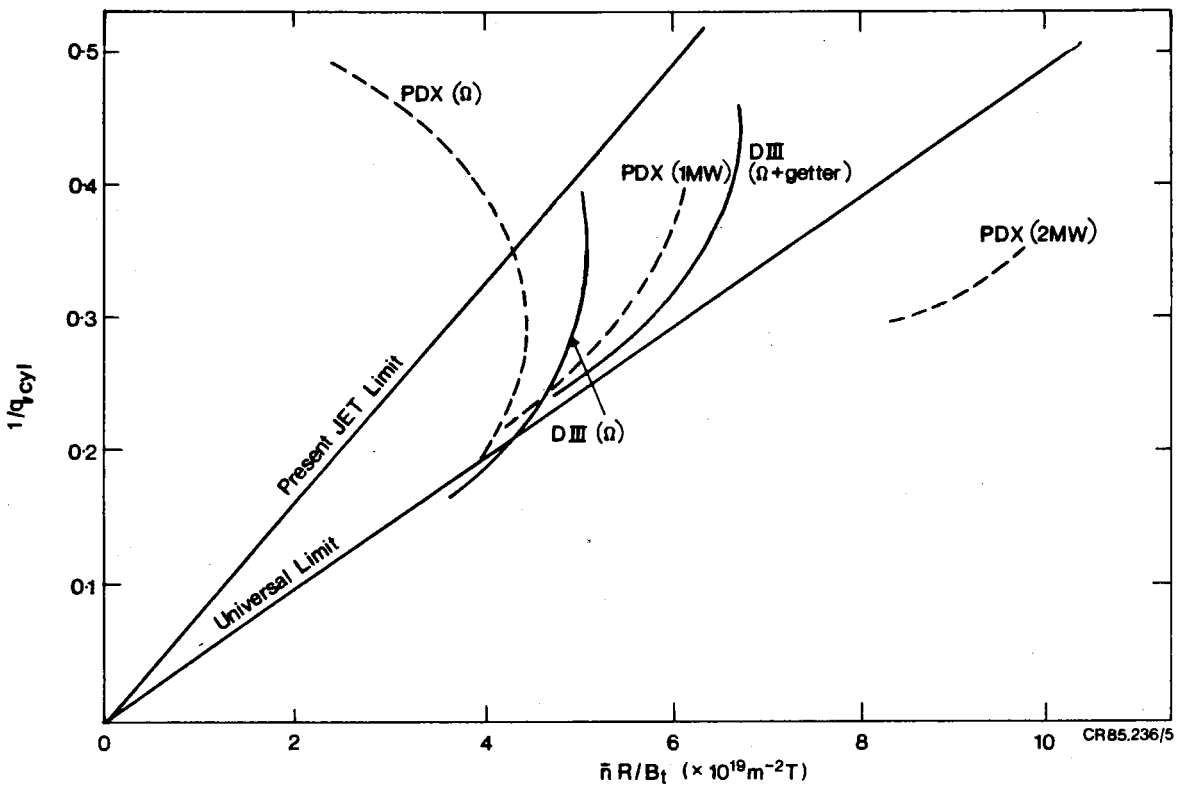

Fig. 10 Hugill-Murakami diagram showing results from JET, PDX and Doublet III (DIII).

P(85)24

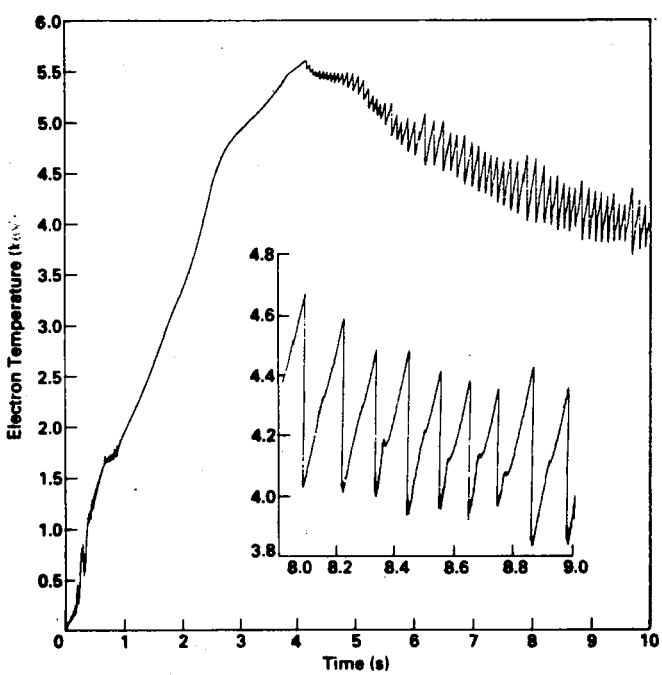

Fig. 11 Central electron temperature behaviour as a function of time (over 10s) showing sawtooth behaviour. The inset shows an expanded timescale (over 8-9s).

P(85)24

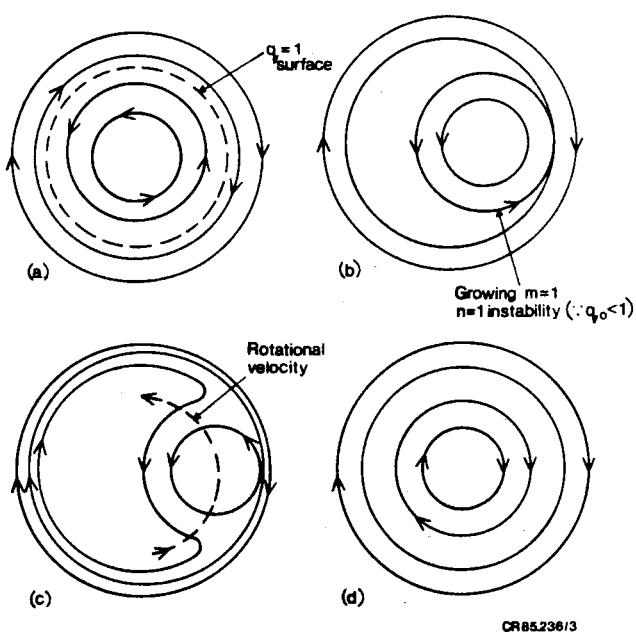

Fig. 12 Transverse field component B^*: (a) initially; (b) when the inner surface touches the outer surface: (c) during reconnection (due to finite resistivity): and (d) after reconnection.

P(85)24

by Kadomtsev (1975). The safety factor at the centre of the plasma q(0) is assumed to be less than unity, so that within the radial region where q = 1, the development of the helical MHD instability mode m = 1/n = 1, is possible. A transverse component of the magnetic field, $B^* = (B_\theta - (r/R)B_\phi) = B_\theta (1-q)$, acting on the perturbation, can have opposite signs on each side of the radial surface, where q = 1. Consequently, due to finite resistivity, reconnection of the field lines can occur as shown schematically in Fig. 12. This "internal disruption" is a violent, large scale convective motion arising from a sudden reconnection of the magnetic field topology, which creates enhanced heat transport within the central region causing the flattening of the profile up to the inversion radius. On a slower timescale, the perturbation relaxes by a diffusive process with a heat conduction coefficient $\chi_e(r)$. Outside the inversion radius, r_s, this effect manifests itself as a heat pulse propagating outwards, which produces the inverted sawtooth seen outside the inversion radius ($q \geq 1$). Consequently, the presence of sawteeth limits the maximum temperature that can be reached in the centre of the plasma and creates a source of energy loss from the central region.

Sawteeth oscillations have been seen in JET from soft X-rays, neutrons, electron temperature, ion temperature and electron density in flat-top discharges for which q_{cyl} at the boundary was less than 12. Fig. 11 shows an example of sawteeth on the central electron temperature as measured by electron cyclotron emission. In many discharges, sawteeth are aperiodic and complex. In a simple case, the sawtooth period τ_{ST} seems to be correlated with the global energy confinement time τ_E and for a particular data set the period of simple sawteeth scales as $\tau_{ST}/\tau_E = 0.13 \pm 30\%$. More commonly, in JET, the behaviour is dominated by giant sawteeth having roughly twice the period of the simple sawteeth (Campbell et al, 1985). This applies particularly when ICRF heating is added. In a certain case, with 2.8MW of RF the central temperature rose from 1.8keV to 3keV, and giant sawteeth developed with amplitude up to 1.8keV.

By using the fast electron cyclotron emission grating polychromator (Tubbing et al,1985) the passage of the thermal wave excited by the sawtooth collapse in the plasma core has been tracked. The observed propagation can be interpreted to give the effective electron thermal

diffusivity $\bar{\chi}_{ep}$ and this can be compared with the value $\bar{\chi}_{eE}$ deduced from the global energy confinement time ($\bar{\chi}_{eE} = a^2/4\tau_E$), typical results from a single shot during RF heating (1.3MW) and after RF, during the Ohmic phase are

	$\bar{\chi}_{ep}$	$\bar{\chi}_{eE}$	$\bar{\chi}_{ep}/\bar{\chi}_{eE}$
RF	$3.5 m^2 s^{-1}$	$1.6 m^2 s^{-1}$	2.2
Ohmic	$3.4 m^2 s^{-1}$	$1.0 m^2 s^{-1}$	3.4

The reason for these differences is not known. A possible explanation is that the equilibrium profile is close to a state of marginal stability and any perturbation causes an enhancement in the thermal loss mechanisms. Another possibility is that there is an inward thermal pinch term analogous to that found for density diffusion.

(c) Impurities

Impurities present a major problem in tokamak plasmas, and have a detrimental effect in that they cause:

(i) a reduction in the number of effective ions in the plasma available for productive fusion interactions;

(ii) large power losses from the plasma by radiation; and

(iii) reduction of the density limit at which major disruptions occur (see section 7(a)).

The parameter which provides a measure of the impurity content of a plasma is the effective ion charge, Z_{eff}, which is defined by the relationship:

$$Z_{eff} = \sum_i (n_i Z_i^2 / n_e) \qquad (11)$$

where the summation is taken over all ions of charge Z_i and density n_i, n_e is the electron density.

One of the main aims of the JET tokamak is to investigate the effects of impurities and the subsequent radiation losses from plasmas, for which visible and VUV spectroscopy, and bolometer and soft X-ray signals are used. O, C, wall metals (Ni, Cr and Fe) and Cl were identified as the main impurities in early JET plasmas. The carbon limiters were the main source of C and the walls appeared to play a dominant role for O impurities. Metals were deposited on the limiter surfaces during the course of operations. Subsequently, limiter sputtering was the main source of metals in the plasma. Metal densities increased with I_p and decreased with plasma density, while light impurities were relatively insensitive to these parameters and depended more on the state of the vessel. This led to the tendency for Z_{eff} to fall with density. During this period, bolometric measurements showed that 70 - 100% of the input power was radiated.

In order to reduce this radiation, a layer of lower Z material, carbon, was deposited on the vessel wall by glow discharge cleaning in a mixture of methane and hydrogen. This reduced the metals content immediately, by about a factor of 5, but this content recovered subsequently as the carbonisation surface was removed or aged. In addition, Cl and O gradually decreased during the carbonisation process, while the C fraction increased. The radiated power dropped as low as 40% and a considerable heat load on the limiters resulted. Due to the reduction of O and Cl, values of Z_{eff} reduced to $\approx$ 2.5, consisting of about 2% C, 1% O, 0.05% Cl and 0.025% metals. The density limit increased marginally, and by removing the remaining O it might increase further.

The effect of the carbonisation on the Hugill diagram is shown in Fig. 8. Carbonisation points are plotted indiscriminately without regard to the carbonization intensity used or the number of pulses after treatment. However, it can be seen that carbonisation extends the density limit by ~ 10%. Fig. 13 shows the radiated power profiles before and after carbonisation for similar plasma parameters. There is a reduction in the power radiated from the plasma core and a narrowing of the annular radiating zone surrounding the plasma.

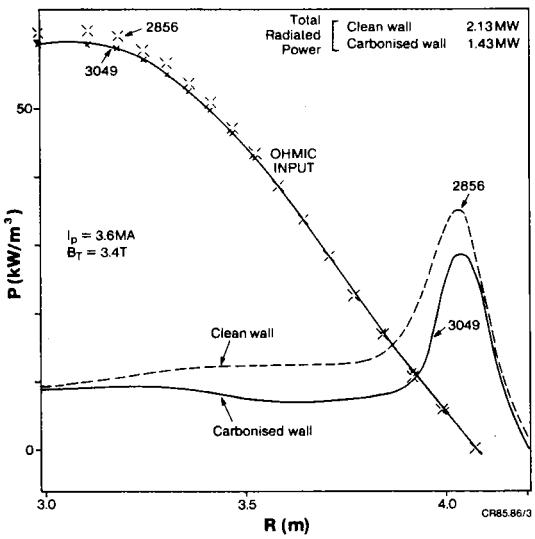

Fig. 13 Input ohmic power, P_Ω, and radiated power, P_{RAD}, profiles for Pulse No. 2856 (before carbonisation) and Pulse No: 3049 (after carbonisation). P(85)24

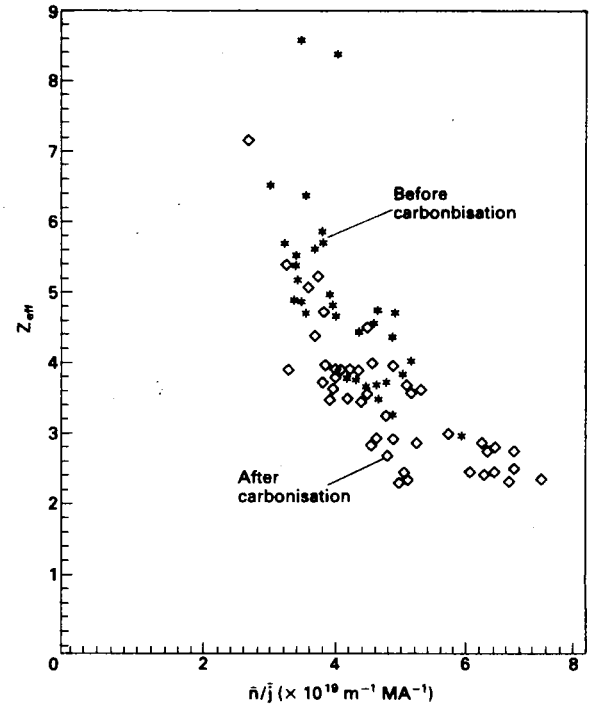

Fig. 14 The effective ion charge Z_{eff}, for bremsstrahlung measurements versus the ratio of average density, $\bar{n}$, to average current density, $\bar{j}$, before and after carbonisation.

P(85)24

Carbonisation is effective in reducing metal concentrations temporarily and oxygen on a longer timescale, but it leads to high carbon concentrations and thus a dilution of the working gas. For Z_{eff} ~3 and a carbon/oxygen ratio of 3:1, about 40% of the plasma electrons originate from impurities. Such depletion can be seen when comparing the neutron yield with the ion temperature from the neutron spectrum. Agreement between the ion temperature deduced from the yield and that measured requires a deuteron/electron density ratio of typically 0.5 in the plasma core. Hydrogen release from the deposited carbon also makes density control difficult in the first few shots after carbonisation. However, carbonisation is the only means found so far for reducing the radiated power once the limiters have become coated with metals.

Fig. 14 shows Z_{eff} from bremsstrahlung measurements versus the ratio $(\bar{n}/\bar{j})$ where $\bar{j}$ is the mean current density in the plasma, and results after carbonisation are distinguished from the rest. It is evident that carbonisation reduces Z_{eff} slightly but that the minimum value is still high at ~ 2.5. To reduce this further in JET, it is planned to surround the plasma more completely with low Z material, i.e. more carbon tiles. Other measures under discussion include gettering with beryllium or chromium and the use of beryllium limiter tiles.

(d) Beta Limits

With the densities and temperatures required in a tokamak fusion reactor ($n = 3 \times 10^{20} m^{-3}$ and $T_e = 10 - 20keV$), a value of the plasma average β (ratio of plasma pressure to magnetic pressure) must be in the range 5 - 10% to provide an economic return on investment in the magnetic field system (Furth, 1981). Higher β values would produce an excessive neutron wall loading in a D-T tokamak. Lower values would drive up the minimum size of reactor.

A key issue for tokamak plasmas is the maximum β that can be contained stably. A number of studies (Troyon et al, 1984, Sykes et al, 1983, etc.) have considered the stability limit for certain MHD instabilities, using optimized pressure profiles that are marginally stable throughout the plasma. A general relationship for the maximum average β value has been found of the form:

$$\beta(\%) = g\ I(MA)/\ B_t(T)\ a(m) \qquad (12)$$

where g is a constant

When ideal MHD ballooning modes only are considered (Sykes et al, 1983) a value of $g = 4$ results, and where ballooning modes and kink modes are present (Troyon et al, 1984), $g = 2.8$. A range of values $g = 2.8 - 4.0$ has been calculated for various configurations with these two main MHD instabilities (Callen, 1985).

The maximum volume averaged β values attained experimentally confirm the theoretical variation with plasma current I_p, toroidal field (B_T) and minor radius, a, and the average value of the constant g is ~ 3.5. This relationship has been observed over a wide range of tokamaks (Doublet III (NBI), PDX(NBI), ASDEX(NBI), TOSCA(ECRH), etc.) in various confinement regimes and at high and low collisionality.

The β-limit can manifest itself either as a strong degradation of confinement ("soft-limit") when β approaches the boundary or as a disruption limit. This degradation has been seen over a wide range of parameters: $q = 1.7 - 7$; $a = 6 - 42cm$; $b/a = 0.95 - 1.6$; $\beta_p = 0.7 - 3.5$; and aspect ratio 3.3 - 5.0. At the "soft-limit", no saturation mechanism has been clearly identified. However, under certain

conditions, modes of the ballooning or kink type have been seen. There are experimental difficulties at high values of β, as such experiments are carried out at low q, high density and high heating power. While the operational beta boundary is close to the theoretically predicted ideal β limit, there is still no clear evidence either that the boundary is an absolute limit or that it is connected with ideal MHD phenomena.

It was suggested that there were potential advantages in using non-circular minor cross-section to raise β-limits (Furth, 1981). However, rigorous analysis (Shafranov and Yurchenko, 1968) based on ideal MHD stability requirements showed that no advantage would accrue with purely elliptical plasmas, and this has been confirmed experimentally. In order to obtain any theoretical benefit, it was necessary to introduce triangularity as well as elongation of the flux surfaces (i.e. a tear-drop shape). Recent experiments on DIII (Stambaugh et al, 1984) have shown that a disruptive limit of $\beta = 3.5\ I(MA)/B_t(T)\ a(m)$ is observed independent of elongation and triangularity. However, the effect of shaping in increasing β came through increasing the plasma current that could be stably operated at given toroidal field, B_t, and minor radius, a, values.
Based on the pessimistic β limit value ($= 2.8\ I(MA)/B_t(T)\ a(m)$), the maximum values for JET are $\beta = 3.5\%$ at 5MA plasma current, and $\beta = 5\%$ at an extended performance value of 7MA. Since this topic is intimately related to energy confinement, it will be considered further in the following section.

8 ENERGY CONFINEMENT

The basic objective of a tokamak device is to confine plasma for a sufficiently long period at attainable density and temperature that the Lawson parameters $\langle n_i \tau_E \rangle$ and T_i can be satisfied in an apparatus of moderate size to be of practical and economic interest. Therefore, the global energy confinement time, τ_E, and how it scales with other plasma parameters is a basic and important property of the device.

Various aspects relating to energy confinement in tokamaks are described in the following sub-sections.

(a) Measurement of τ_E

τ_E is derived from the equilibrium relationship,

$$\tau_E = (W_e + W_i)/P_{in} \qquad (13)$$

where $\left(W_e = \frac{3}{2} \int n_e T_e \, dV\right)$ and W_i $\left(= \frac{3}{2} \int n_i T_i \, dV\right)$ are the electron and ion energies, respectively and P_{in} is the total input power to the plasma. Calculation of τ_E requires knowledge of the density and temperature profiles for both electrons and ions and the extent of plasma surfaces. [In the case of JET, the $n_e(r)$ profile is obtained from the multi-channel interferometer; $T_e(r)$ profile from ECE measurements; T_i from NPA, and the assumption that the profile shape follows $T_e(r)$; n_i/n_e from neutron yield/spectrum or from spectroscopy; and plasma surfaces from magnetic measurements and relevant calculations.]

For Ohmic heating, the power input for equilibrium cases is simply $P_\Omega = I_p V$ where V is the loop voltage; for non-equilibrium cases, there must be a correction for the inductive contribution. With additional heating, the measurement of τ_E is more complex. In principle, it is possible to modulate the additional heating source (RF or NBI) and study the plasma reaction $\left(d(W_e + W_i)/dt\right)$ following the switch-on or switch-off of the source. Then, the transient situation is described by:

$$\frac{dW}{dt} = \Delta P_{in} - \Delta L$$

where W is the plasma energy, and L is a loss term.

However, if $\tau_E = f(P_{in})$ or $\tau_E = f(E)$, then calculation is complicated and different values of τ_E ensue.

In JET, with ICRF additional heating, it is assumed that all launched RF power is absorbed by the plasma, which results in a lower limit for the τ_E value.

(b) Scaling Laws

From the early work on tokamaks, efforts have been devoted to establishing empirical scaling laws connecting τ_E with other plasma parameters. Early work is reviewed by Bickerton (1977).

There are doubts about the relevance of the parameter τ_E, since it is averaged over a volume including the central sawtooth instability zone, the confinement zone (between q = 1 and q = 2) and the outer radiating zone (edge plasma). Nevertheless, regression analyses have been performed on confinement data, in which scaling laws are postulated, of the form:

$$\tau_E = kA^{\alpha}B^{\beta}C^{\gamma}..... \qquad (14)$$

where A, B, C,... are variables and α, β, γ, ... are determined by fitting to data.

In many cases, there are constraints imposed by relationships between some of the variables A, B, C, etc. In some cases, the range of parameter variation is rather limited, and finally there is no physical basis for a power law relationship (N.B: firmly based physical models of confinement, such as classical and neo-classical transport, do not give power laws.)

An extensive exercise was carried out by Goldston (1984) who considered data from many tokamaks over a wide range of paramters to obtain scaling laws as follows:

(i) Low density Ohmic regime:

$$\tau_E(s) = 7.1 \times 10^{-22}\, n_e(cm^{-3})\, a^{1.04}(cm)\, R^{2.04}(cm)\, q^{0.5} \qquad (15)$$

(ii) High density Ohmic regime:

$$\tau_E(s) = 51\, R^{1.8}(cm)\, a^{-0.9}(cm)\, I^{3/14}(A)\, Z_{eff}^{3/7}\, n^{-3/7}(cm^{-3}) \qquad (16)$$

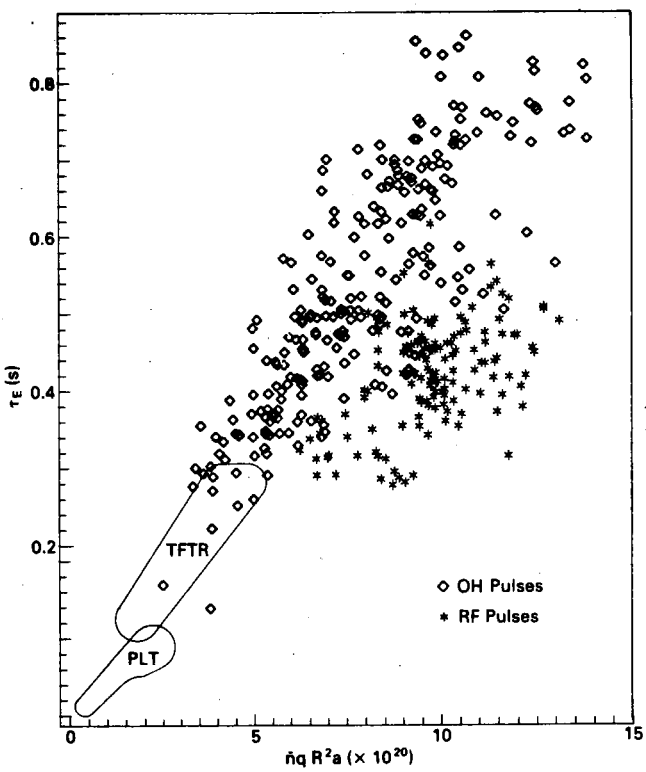

Fig. 15 Global energy confinement, τ_E, versus the scaling factor $\bar{n}qR^2a$ for both ohmic and RF heated plasmas in JET. The data from PLT and TFTR are shown for comparison.

P(85)24

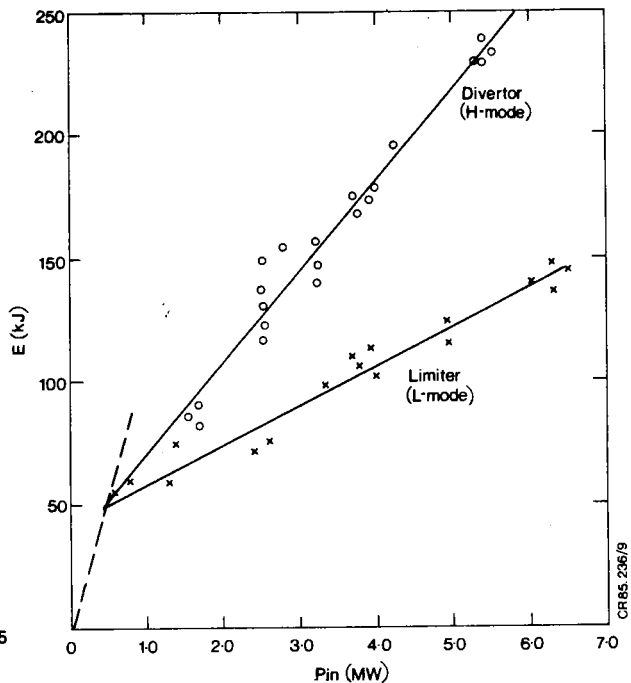

Fig. 16 Plasma energy E(kJ.) as a function of total input power P_{in} for limiter and divertor discharges with additional NBI heating—Doublet III. (Note: $\tau_E \propto E/P_{in}$).

P(85)24

(iii) Additional heating (L-mode) regime:

$$\tau_E(s) = 6.4 \times 10^{-8}\ I_p(A)\ P_{tot}^{-1/2}(W)\ R^{1.75}(cm)\ a^{-0.37}(cm)\ K^{1/2} \quad (17)$$

However, Ohmic heating results for TFTR, PLT, PDX and early values from JET (1984) gave a relationship consistent with the scaling law:

$$\tau_E \alpha \bar{n}qR^2a \quad (18)$$

Fig. 15 shows a plot of <u>all</u> the latest JET data (including ICRF additional heating and with carbonized walls) on this scaling law basis. It seems that the more recent JET results (with additional RF heating and with carbonized walls) no longer fit this scaling law, and now fit a relationship of the form:

$$\tau_E \alpha (\bar{n}B_t)^{1/2}\ q^{1/3}\ K^{1/2} \quad (19)$$

where K = b/a is the elongation factor.

Due to the complications of edge plasmas and interactions with limiters, it is sometimes instructive to consider plasma inside this edge region. A refinement of the global energy confinement time τ_E, is then a surface value of the global confinement time, τ_ψ, which is the energy confinement time inside a specific flux surface. This is given by:

$$\tau_\psi = \frac{\frac{3}{2}\int_0^\psi (n_e T_e + n_i T_i)\, dV}{P_\psi} \qquad (20)$$

where P_ψ is the power input to the plasma inside the surface, ψ, which can be obtained from magnetic measurements in the Ohmic heating case (with additional heating the same problems still apply). Generally, in JET, τ_ψ has a flat maximum ~ $1.3\tau_E$ in the central plasma core.

It should be emphasised that the observed confinement times are always significantly less than those expected from the theory of plasma transport based on binary collision phenomena. This difference is believed to be due to a saturated level of plasma turbulence in the plasma interior, since the plasma is always unstable according to linearised analysis. Definitive experimental evidence on the nature of this turbulence is still lacking due to the difficulty of measuring fluctuating parameters inside a hot plasma.

(c) Confinement Degradation

With additional heating the Goldston (L-mode) scaling law relationship shows that the confinement time, τ_E, is proportional to $P_{tot}^{-1/2}$, and so degradation of τ_E is predicted with increased power. This relationship has been confirmed in a number of experiments, including JET with ICRF heating. In particular, the scaling with $P_{tot}^{-1/2}$ is observed and the absolute value agrees well with predictions. [i.e. at I_p = 2.8MA; P_{tot} = 6MW; K = 1.5; the measured value is τ_E = 0.33s compared with the predicted Goldston (L-mode) value of τ_g = 0.33s.]

However, in spite of this early poor performance with additional heating, a good confinement regime with neutral beam heated plasmas was observed in ASDEX, PDX and Doublet III tokamaks. This is the so-called H-mode of operation which occurs in tokamaks with a magnetic limiter or divertor, and which is characterized by a high electron temperature near

the seperatrix and a steep gradient indicating very much reduced radial transport compared with the L-mode. The L to H mode transition is often triggered by a sawtooth heat pulse. A further feature is that the transition is signalled by a reduction in edge recycling of neutral hydrogen.

In the H-mode, the energy confinement time $\tau_E(H)$ is typically 2 - 3 times greater than the corresponding L-mode value, τ_g. Obviously, this is a desirable feature in any plasma confinement device. Typical results obtained in Doublet III (Burrell et al, 1985) are shown in Fig. 16. This shows the total energy stored in the plasma, E, versus the total power input, P_{in}, to the plasma during NBI experiments both in limiter (L-mode) experiments and in divertor (H-mode) exeriments. The energy confinement time τ_E ($\propto E/P_{in}$) shows a substantial increase when a divertor is used.

However, the conventional type of magnetic divertor takes up considerable space and a new type of divertor-like magnetic field configuration has been found to improve plasma confinement. This is called an Expanded Plasma Boundary in which a magnetic separatrix (or X point) is located inside the vessel wall, removing the effective outer flux surface away from the limiter. The configuration of poloidal field coils on JET allows the formation of a separatrix with two stagnation (or X) points, at the top and bottom of the vacuum vessel. Experiments with Ohmic heating only have been carried out to demonstrate this mode of operation and to study a number of technical questions relating to the up-down stability and heat loads on the vessel (Tanga et al, 1985). Fig. 17 shows the flux contours of such a case at I_p = 2MA, B_t = 2.6T. The configuration was maintained stably for several seconds and interaction with the mid-plane limiters stopped. It is beleieved that JET can operate for several seconds at current levels of 4MA without modifications to existing poloidal field coils. Experiments are continuing.

A crucial question relating to H-mode discharges is what happens as the theoretical β-limit is approached. If improved H-mode confinement persisted at low B_T and high beam power, the beta values obtained in L-mode (limiter) discharges should be exceeded by up to a factor of two, despite even an L-mode power scaling of $\tau_E \propto P_{tot}^{-1/2}$. However, it was

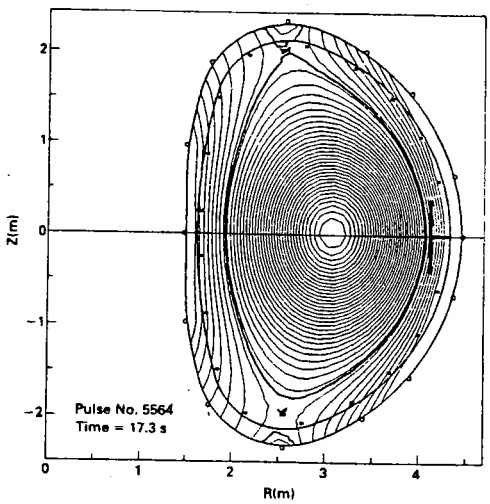

Fig. 17 Pulse No. 5564: (I_P=2MA, B_t=2.6T) showing formation of magnetic separatrix inside the vacuum vessel.

P(85)24

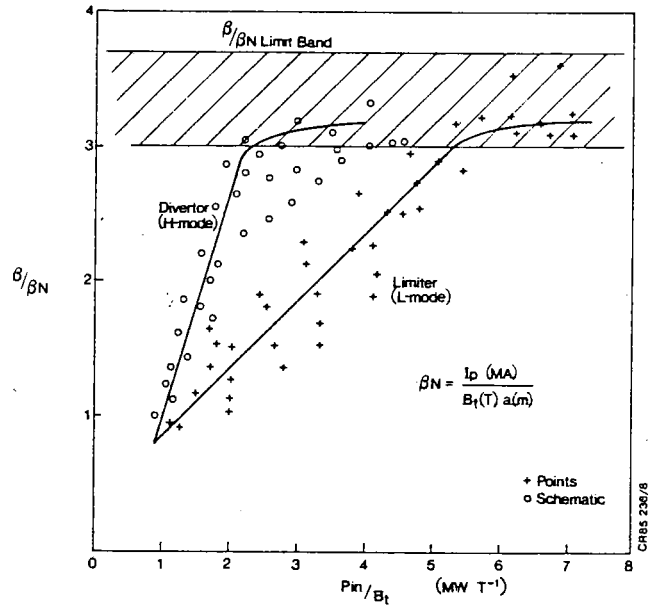

Fig. 18 Plot of β/β_n [$\beta_n = I_p(\mathrm{MA})/B_t(\mathrm{T})a(\mathrm{m})$] versus the ratio of total input power (P_{in}) to toroidal magnetic field (B_t) in NBI heated plasmas in PDX.

P(85)24

found in PDX that τ_E fell precipitously and β saturated as beam power was increased. In part, this may have been due to the strong gas feed required to avoid disruptions in PDX under these circumstances, since a large gas feed was shown to destroy the enhanced H-mode confinement. However, the disruptions themselves may have been the sign of the β-limit; they are avoidable only by reducing τ_E (and thus β) through spoiling the H-mode confinement. This situation is shown in Fig. 18 when it seems that in either the H or L mode regimes the β-limit is given by $\beta(\%) = 3.5\ I_p(\mathrm{MA})/B_t(\mathrm{T})a(\mathrm{m})$. However, this situation is worthy of further analysis. Even so, the H-mode is advantageous in that the β-limit is reached for reduced additional power input at a fixed toroidal magnetic field.

(d) Importance of τ_E and β

In a reacting plasma, the thermal (α-particle) power produced per unit volume is:

$$P_{th} \propto n^2(\bar{\bar{\sigma v}})Q.$$

where $(\bar{\bar{\sigma v}})$ is the product of the cross-section for reaction and the velocity averaged over a Maxwellian distribution and Q is the energy release per reaction.

However, for a D-T reaction, $(\overline{\sigma v}) \propto T^2$ (for T in the range of an anticipated reactor, i.e. 7-15keV). Therefore $P_{th} \propto n^2T^2$. If P_{in} is the input power to the reactor,

$$P_{in} \propto nT/\tau_E \tag{21}$$

Therefore, $$\frac{P_{th}}{P_{in}} \propto \frac{n^2T^2\tau_E}{nT} \propto nT\tau_E$$

but $$\beta \propto nT$$

Consequently, $$\frac{P_{th}}{P_{in}} \propto \beta\tau_E \tag{22}$$

This shows that it is important to obtain maximum values of β and τ_E for optimum α-heating. Using parameters anticipated during JET's full performance (i.e. B_t = 3.5T; Plasma volume = 150m^2; P_{in} = 35MW; Plasma energy, $E = 2/3\ (n_iT_i + n_eT_e) = 11\beta(\%)$MJ (for a depletion factor $\gamma = n_i/n_e = 1$); $P_\alpha = \gamma^2\beta(\%)^2$), α-power heating and corresponding confinement times may be calculated. These are shown in Table 4, where $\tau_{E1} = E/P_{in}$ and $\tau_{E2} = E/(P_{in} + P_{th})$. These calculated confinement times are compared with those expected on the Goldston additional heating (L-mode) scaling law. The pessimistic β-limit (Troyon,1984) is $\beta_c = 2.8I_p(MA)/B_t(T)a(m)$, which gives values of 3.5% (at I_p = 5MA) and 5% at I_p = 7MA (enhanced performance). Table 4 shows that if a β value of 5% (i.e. at I_p = 7MA) can be obtained, substantial α-heating should be achieved on JET. However, this would require confinement times three times greater than that predicted by Goldston L-mode scaling.

TABLE 4

$\beta(\%)$	I_p(MA)	E(MJ)	P_α(MW)	τ_{E1}(s)	τ_{E2}(s)	τ_g(s)
1	5	11	1	0.31	0.31	0.29
2	5	22	4	0.63	0.56	
4	5	33	9	0.94	0.75	0.25
4	7	44	16	1.26	0.86	0.32
5	7	55	25	1.57	0.92	0.30

Note: τ_g = Goldston L-mode scaling (including α-power).

9 ACHIEVEMENTS

The main achievements with tokamak devices may be summarised as follows:

(a) The underlying tokamak magnetic field configuration can be set up and equilibrium maintained stably for long periods over a wide range of machine sizes and parameters;

(b) The new range of larger machines (JET, TFTR, JT-60,...) behave in a similar fashion to the smaller original tokamaks, particularly in formation of the discharge and subsequent behaviour of the plasma;

(c) Long duration discharges have been obtained in JET (up to 20s), without disruptions even during the current decay. However, the density limit (determined by the disruption boundary) is low, at present, and further efforts, especially during additional heating will be needed to extend this limit;

(d) The expected advantage of increased size is seen with all the larger machines. In particular, in JET a record confinement time $\tau_E = 0.8$s has been seen;

(e) High electron and ion temperatures have been produced in Ohmically heated plasmas. Values of $\hat{T}_e$ up to 5keV and $\hat{T}_i$ up to 3keV have been produced in JET, with inputs of less than 3MW, although Z_{eff} was in the range 2.5 - 8;

(f) Additional heating in the MW's range has been coupled or injected into tokamak plasmas from RF sources and from neutral beam injectors. Substantial ion and electron heating has resulted (with ion temperatures approaching the 10keV needed to meet the Lawson criterion), although there has been associated confinement degradation. Further efforts will be needed to circumvent this problem;

(g) There are still problems associated with MHD instabilities which manifest themselves as major disruptions and sawteeth oscillations, thus limiting the maximum densities and temperatures that can be reached. These problems must be surmounted in order to reach the necessary Lawson parameter values;

(h) Impurities still create difficulties. In early JET experiments, high levels of radiated power resulted from metal impurities at the centre and low-Z impurities at the edge. Later experiments with

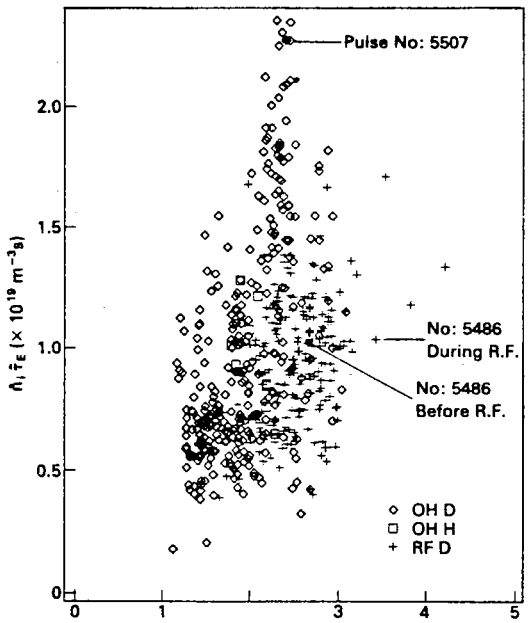

Fig. 19 Lawson diagram of $\langle \hat{n}_i \hat{\tau}_E \rangle$ versus $\hat{T}_i$(NPA) for both hydrogen (H) and deuterium (D) plasmas during ohmic and RF heating. Pulse No: 5507 and Pulse No: 5486 (both before and during RF heating) are highlighted.

P(85)24

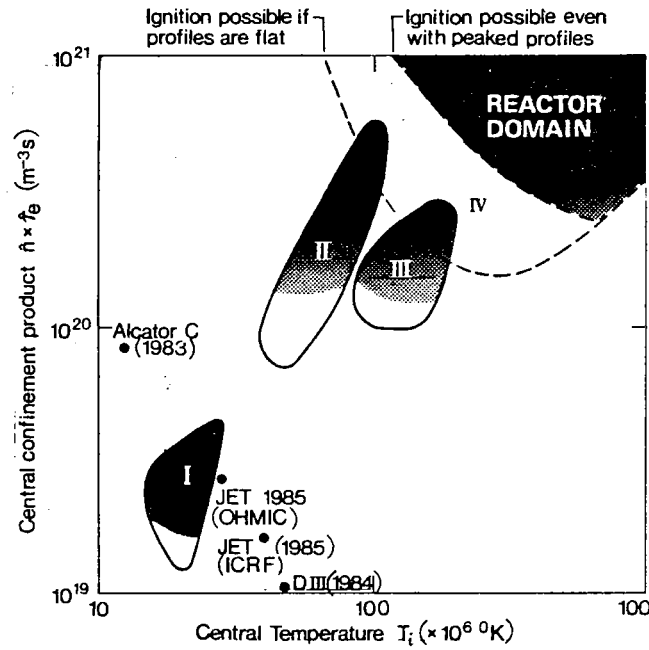

Fig. 20 Lawson diagram showing predicted results for different phases of JET operation. Phase I corresponds to ohmic heating power only; Phase II to additional heating of ~20MW; Phase III to additional heating of ~35MW: to operation in D-T mixtures based upon various theoretical models (see Gibson, 1984).

P(85)24

carbonised walls showed reduced levels of metals, lower Z_{eff} values and decreased radiation losses. However, there is still an ion depletion problem;

(i) With respect to the gross parameters required to meet the Lawson criteria (i.e. $\hat{T}_i$ = 10keV, $\langle \hat{n}_i \hat{\tau}_E \rangle = 3 \times 10^{20} m^{-3}$), the highest central ion temperature in JET - 4.5keV has been achieved with ICRF heating, and with Ohmic heating, $\hat{T}_i$ = 2.6keV and $\langle \hat{n}_i \hat{\tau}_E \rangle = 2.5 \times 10^{19} m^{-3}s$ has been obtained (see Fig. 19).

10 FUTURE OUTLOOK

Of the larger tokamaks planned worldwide (see Table 2), TFTR (USA) started operation in December 1982, JET (EEC) in June 1983, and JT-60 (Japan) in April 1985. Further, T-15 (USSR) and DIII (USA) are due to operate in 1986, and TORE-SUPRA (France) and FT-U (Italy) are due in 1987. Of these machines, only TFTR and JET are designed to operate eventually in D-T mixtures. The present status of achieved gross parameters are shown in Fig. 20, together with the predicted performance for JET based upon theoretical calculations. Phase I corresponds to

predictions during the ohmic heating phase only; Phase II relates to additional heating up to ~20MW and Phase III to additional heating up to the planned total of ~35MW, for operation in hydrogen and deuterium plasmas. Phase IV corresponds to operation in D-T mixtures with the full ohmic and additional heating power, under favourable conditions (Gibson, 1984).

In relation to the JET machine, the outlook is as follows:

ICRF Heating has already been tested on JET at generator levels of 6MW (5MW coupled to the plasma from 2 antennae), without major impurity problems. Substantial ion and electron heating has already been observed at this level. The ICRF heating system will be progressively upgraded both in power and in antenna design. There are several modes of heating, working either at the fundamental frequency of a minority species considered (e.g. ^{3}He in H and D in H), or at harmonic of the main ion species. The system frequency range (25 to 55 MHz) covers the different modes for the plasma species considered (D, H, T, ^{4}He and ^{3}He). By 1986, the present two experimental antennae will be replaced by three with 9MW from the generators. Later, a total of eight antennae, with 32MW from the generators (at least 15MW in the plasma), should be available.

The first neutral beam injector designed to deliver 5MW of 80keV neutral hydrogen particles into the plasma will operate in 1985. The injector contains 8 ion sources, and ion beam pulses of 80keV and 60A have been produced according to specification. Beam heated plasmas should be produced in late 1985. Manufacture of all components for the second injector is well advanced and this should be installed in 1987. It is planned to change to deuterium later, and a prototype source has already produced a beam of 160keV deuterons to the required specification.

With this large additional power applied to JET plasmas, substantial ion and electron heating should result. Its effect on confinement and production of plasma impurities will be monitored closely.

In conclusion, it should be noted that significant progress has already been made with the present breed of large tokamaks. Further, experiments performed during the next 5-10 years with substantial additional heating should well answer questions on whether density limits, β limits, confinement degradation and impurity problems can be surmounted in the tokamak configuration.

11 REFERENCES

Alikaev,V.V., et al, Proc of 10th IAEA Conf on Plasma Physics and Controlled Nuclear Fusion Research,Vol.2,p.419, (1984)

Artsimovich,L.A., Nuclear Fusion 12, 215 (1972)

Bickerton,R.J., (1977) Theory of Magnetically Confined Plasmas (Varenna, Italy. Eds. Coppi,B. et al) EEC/Pergamon Press. p.423.

Bol K et al (1974), Proc. 5th IAEA Conf. on Plasma Physics and Controlled Fusion Research, vol.1,p.387.

Burrell,K.H., et al (1985) Proc of 10th IAEA Conf on Plasma Physics and Controlled Fusion Research (London, UK, 1984). Vol II, p.131

Campbell D J et al, Proc. 12th European Conf on Controlled Fusion and Plasma Physics (Budapest, Hungary, 1985) Vol.9F,Part 1,p.130. Callen,J.D., (1985) Proc of 10th IAEA Conf on Plasma Physics and Controlled Nuclear Fusion Research (London, UK, 1984). Vol 3, p.473

Cima G et al (1976) Proc. 6th IAEA Conf. on Plasma Physics and Controlled Fusion Research, Vol.1,p.335.

Furth,H.P., Nuclear Fusion 15, 487 (1972)

Furth H P,(1981) in Fusion: Vol.1 Magnetic Confinement (Academic Press, NY.USA) p.124

Gibson A, Proc. 1984 Int. Conf. on Plasma Physics, (Lausanne, Switzerland) Vol.1,p.13 (1984)

Goncharev S G (1984), Proc. of 10th IAEA Conf. on Plasma Physics and Controlled Nuclear Fusion Research, Vol.1,p.77.

Goldston, T.J., (1984), Plasma Physics and Controlled Fusion, 26, 87

Jacquinot,J., et al, Budapest EPS Conference (1985)

JET Report, EUR-JET-R5, Commission of the European Communities, Brussels, (1975)

Kaganski M G , et al (1976), Proc. 6th IAEA Conf. on Plasma Physics and Controlled Fusion Research, Vol.1,p,217.

Kitsunezaki,A., et al, Proc of 10th IAEA Conf on Plasma Physics and Controlled Nuclear Fusion Research, Vol.1, p.57, (1984)

Laing E W, Roberts S J and Whipple R T P, (1959) Plasma Physics,1,49.

Little R and Rawls J M (1984) Nuclear Fusion, 24 657.

Poincarré,H., J. Math.(1881-85)

Porkolab,M., et al, Proc of 10th IAEA Conf on Plasma Physics and Controlled Nuclear Fusion Research,Vol.1,p.463, (1984)

Shafranov V D and Yurchenko E I (1968) Nuclear Fusion, 8, 329

Spitzer L (1956) Physics of Full Ionized Gases (J Wiley, New York)

Stambaugh R D et al (1976) Proc. 10th IAEA Conf. on Plasma Physics and Controlled Fusion Research, Vol.1,p.217

Stott,P.E., et al (Eds) Diagnostics for Fusion Reactor Conditions (Varenna, Italy, 1982) EUR-8351-EN

Sykes,A., Turner,M.F., Patel,S., Proc. of 11th European Conf. on Controlled Fusion and Plasma Physics (Aachen, 1983). Vol 7D, Part II, p. 363(1983)

Tait G et al (1984) Proc. of 10th IAEA Conf. on Plasma Physics and Controlled Nuclear Fusion Research Vol.1,p.141.

Tamm,I.E., Plasma Physics and Problems of Controlled Thermonuclear Fusion, I, 3 Acad. Nauk (USSR), (1958)

Tanga,A.,et al Proc 12th European Conference on Controlled Fusion and Plasma Physics (Budapest, Hungary, 1985) Vol 9F, Part 1,p. 70

Tubbing B J D, et al Proc. 12th European Conf. on Controlled Fusion and Plasma Physics (Budapest, Hungary, 1985) Vol9F,Part1,p.130.

Troyon,F., Gruber,T., Saurimann,H., Semenzato,S., Succi,S., Plasma Physics, 26, 209(1984)

World Survey of Major Activities in Controlled Fusion Research, IAEA, Vienna (1982)